

Many-body localization in Ising models with random long-range interactions

Haoyuan Li*

Department of Physics, Tsinghua University, Beijing 100084, China

Jia Wang, Xia-Ji Liu, and Hui Hu†

Centre for Quantum and Optical Science, Swinburne University of Technology, Melbourne 3122, Australia

(Dated: February 15, 2021)

We theoretically investigate the many-body localization phase transition in a one-dimensional Ising spin chain with random long-range spin-spin interactions, $V_{ij} \propto |i - j|^{-\alpha}$, where the exponent of the interaction range α can be tuned from zero to infinitely large. By using exact diagonalization, we calculate the half-chain entanglement entropy and the energy spectral statistics and use them to characterize the phase transition towards the many-body localization phase at infinite temperature and at sufficiently large disorder strength. We perform finite-size scaling to extract the critical disorder strength and the critical exponent of the divergent localization length. With increasing α , the critical exponent experiences a sharp increase at about $\alpha = 1$ and then gradually decreases to a value found earlier in a disordered short-ranged interacting spin chain. For $\alpha < 1$, we find that the system is mostly localized and the increase in the disorder strength may drive a transition between two many-body localized phases. In contrast, for $\alpha > 1$, the transition is from a thermalized phase to the many-body localization phase. Our predictions could be experimentally tested with ion-trap quantum emulator with programmable random long-range interactions, or with randomly distributed Rydberg atoms or polar molecules in lattices.

PACS numbers: 75.10.Pq, 05.30.Rt, 72.15.Rn

I. INTRODUCTION

Many-body localization (MBL) phase transition [1–3] is an interesting phenomenon and has caught huge attention of physicists in various perspectives. From a theoretical point of view, this localization phenomenon addresses one of the most fundamental problems in statistical mechanics: How does a generic quantum many-body system evolve, when it is absolutely isolated from environment? The fundamental Schrödinger equation governing the dynamics of a quantum system is a linear equation, which renders the traditional explanations of thermalization, i.e., via ergodicity and equilibrium states, inapplicable [4, 5]. Besides attempting to adapt the original concepts and methods to new situations [6, 7], during the last several decades, another extensively explored approach is to establish an alternative hypothesis. The eigenstate thermalization hypothesis (ETH) [8–10] is one of the most successful hypotheses. It asserts that in a generic quantum many-body system, for nearly every highly excited eigenstate, averaging thermodynamic observable over that eigenstate essentially leads to the classical equilibrium value. This hypothesis results in significant implications and profound insights into the thermalization process and was proved to be equivalent to an crucial assumption, i.e., the von Neumann’s quantum ergodic theorem [6, 7]. However, to some extent, one of the most important prospects of this hypothesis

is to provide a manipulable criterion to characterize the breakdown of equilibrium statistical mechanics.

Anderson localization (AL) phase transition in non-interacting systems [11, 12] proves that it is an oversimplified picture in ETH to assume that equilibrium states always exist. As a natural analogy of AL phase transition in interacting systems, MBL phase transition pushes the inquiry of the boundary of that picture to a new realm: Can strong enough quenched disorder localizes a generic quantum many-body system, or at least breaks the eigenstate thermalization hypothesis? Exploring such profound questions will lead to a deeper understanding of the non-trivial role of interactions and disorder in evolutions of many-body systems and fundamental concepts of statistical mechanics, such as temperature, ergodicity and extensiveness in quantum statistical mechanics and phase transition.

This topic has attracted huge interest ever since Anderson’s seminal paper [11] on AL phase transition. Anderson himself already showed interest in extending the localization phase transition concept to systems with interactions. He and many successors have tried to prove the existence of the localized phase in interacting models. (For recent reviews, see for example, Refs. [2] and [3].) Thanks to their efforts, many exotic features of the MBL phase and phase transition have been discovered: the existence of the mobility edge [13–15], vanishing of conductivity at non-zero temperature in the MBL phase [16–18], existence even with weak connection to thermal bath [19], sustaining long-range order in situations where equilibrated systems would not [20–24], half chain entanglement entropy of (highly excited) eigenstates obeying an area-law [21, 25, 26], possessing an extensive number

* Chris.Lee.China.1993@gmail.com, present address: Department of Physics, Stanford University, Stanford, California 94305, USA

† hhu@swin.edu.au

of local integral motions [27] and universal slow growth of entanglement of eigenstates after a sudden quench [24, 25, 28–30]. These features are also taken as indicators for the MBL phase.

From an experimental (and engineering) point of view, MBL phase and phase transition are also of great interest and importance. Localization implies that the information stored through local freedom within the initial state will remain within local freedoms [31]. This may help to develop future quantum devices for quantum information process [2, 3]. In addition, the rapid progress of cold atom experiments over the past two decades has immensely expanded our ability to control the experimental conditions for studying quantum physics [32]. Especially in a dilute quantum gas with or without optical or magnetic lattice, we can induce different forms and tune the strength of interactions to a large extent at our will [33]. This makes the direct observation and simulation of quantum many-body systems possible [34]. Experimental exploration is now one of the most promising approaches towards this phenomenon, with several experiments successfully implemented, including both neutral atom gas systems [35–37] and ion traps [38]. Both short-range interaction and long-range interaction have been realized. On the other hand, because of the quantum nature of many-body systems, theoretical study of MBL phase transition is in general quite challenging.

At present, in the extensive literature, three kinds of theoretical approaches are most popular to tackle the MBL challenge: resonance analysis [39–42], renormalization group methods [10, 29, 42–46] and numerical exact diagonalization [13–15, 18, 27, 28, 47–50]. Each method has its own pros and cons. Resonance analysis and renormalization group can be applied to relatively large systems. However, it is challenging to justify the validity of these approaches. On the other hand, numerical exact diagonalization is reliable but can only handle rather small systems.

All of these approaches has been applied for systems with short-range interactions, such as Heisenberg model [13, 14, 18, 25] and Ising model [24, 26, 53]. Nevertheless, there have been only few numerical studies on systems with long-range interactions that might be of more interest for experimentalists, including trapped ions, Rydberg atoms, and polar molecules with dipole-dipole interactions [38, 40, 42, 51, 52, 54, 55] where the MBL physics in these systems is less understood. Using long-range interacting spin chains under random transverse fields as an example, it has been recently suggested that the spin-spin interaction in the form of $V_{ij} \propto |i - j|^{-\alpha}$ always leads to the breakdown of the localization in the thermodynamic limit when $\alpha < \alpha_c$, where α_c is a threshold interaction exponent that depends on the dimensionality d of the system. By constructing hierarchical spin resonances [40], one obtains $\alpha_c = 2d$ for the Heisenberg and Ising models [51] and $\alpha_c = 3d/2$ for the XY model [52]. However, this picture of the so-called interaction-assisted delocalization is not unambiguously settled. For a one-dimensional (1D)

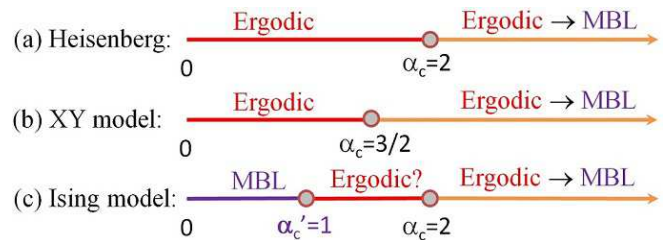


FIG. 1. (color online). Proposed phase diagrams of 1D long-range interacting spin models under random magnetic fields in the thermodynamic limit: (a) the Heisenberg model [40, 51], (b) the XY model [52] and (c) the Ising model [42, 51]. For all three spin models, it was predicted that the system is delocalized and ergodic when $\alpha < \alpha_c$; while for $\alpha > \alpha_c$ the system experiences a transition from the de-localized state to the many-body localization state with increasing disorder strength. For the Ising model in (c), an additional many-body localization phase is suggested to appear at any nonzero disorder strength when $0 \leq \alpha \leq \alpha'_c = 1$ [42].

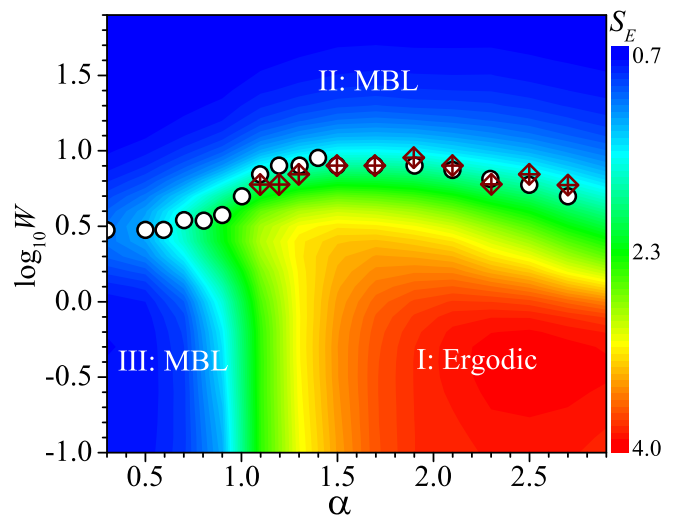


FIG. 2. (color online). Contour plot of the half-chain entanglement entropy of a $L = 14$ Ising spin chain with random long-range interactions (see the Hamiltonian Eq. (1)) at infinite temperature, as functions of the interaction exponent α and the disorder strength W (in the logarithmic scale). A thermalized phase (I) and two many-body localization phases (II and III) are clearly visible. The symbols show the phase boundary determined from the finite scaling of the entanglement entropy (circles) and of the energy spectral statistics (diamonds). Here, we take a uniform transverse $B = 0.6J$.

transverse-field Ising chain, an additional many-body localization phase has been shown by Hauke and Heyl to occur at $0 \leq \alpha \leq 1$, using both numerical simulation and non-equilibrium dynamical renormalization group analysis [42]. The various proposed phase diagrams of 1D disordered long-range spin chains are briefly summarized in Fig. 1.

This work aims to shed some light on settling the above-mentioned debate, by performing extensive numer-

ical calculations via exact diagonalization for a specific Ising model with disordered long-range interactions. Our main results are summarized in Fig. 2, which reports the half-chain entanglement entropy (S_E) of our Ising model with length $L = 14$. One may easily identify an ergodic, thermalized phase and two MBL phases. The phase boundary between ergodic and MBL phases has been determined by a finite-size scaling analysis. Our results strongly support the conclusion by Hauke and Heyl that there is an MBL phase at any nonzero disorder strength in the long-range Ising chains at $0 \leq \alpha \leq 1$, in spite of the fact that in our model the disorder is implemented in long-range interactions, in a way quite different from the traditional method in the literature, i.e., through random transverse field [40, 53] or random potential [13, 14, 25, 42, 47, 56]. Our results seem to rule out the possibility of interaction-assisted delocalization at $1 < \alpha < 2$, as predicted by the resonant spin-pair-excitation argument [40, 51]. On the other hand, it is worth noting that, our Ising model might be realized with the trapped ion quantum emulator [38] or randomly distributed Rydberg atoms or polar molecules in lattices, and thus our results may stimulate new directions for further experiments.

II. NUMERICAL SIMULATIONS

A. The model Hamiltonian

We consider the following Ising model with disordered long-ranged interactions, described by the model Hamiltonian with open boundary condition,

$$\mathcal{H} = J \sum_{1 \leq i < j \leq L} \frac{(1 + h_i h_j)}{|j - i|^\alpha} \sigma_i^z \sigma_j^z + B \sum_{i=1}^L \sigma_i^x, \quad (1)$$

where σ_i^x and σ_i^z are the Pauli matrices representing the i -th spin in the spin chain with L spins. B is a uniform transverse field and $J = 1$ sets the energy unit of the model. The exponent α characterizes the range of interactions, where a larger α implies a shorter interaction range. $\{h_i\}$ is a set of L independent dimensionless random variables, with uniform distribution in the domain $[-W, W]$, where W is defined as the *dimensionless* disorder strength. Alternatively, one may replace $h_i h_j$ with a single variable h_{ij} that distributes uniformly in some intervals; but the results should not change qualitatively. Here, the disorder enters into the system entangling with the long-range interaction in a non-trivial way. In the previous work [42], the renormalization group analysis reveals that through renormalization, disorder on the transverse field induces effective disorder on interactions. However, theoretical investigations into models with disorder on interactions are relatively rare. Therefore, a directly simulation of Eq. (1) can to some extent provide theoretical predictions for the behavior of system with quenched disorder on *interactions* and thereby

testify the universal MBL physics in an entirely new situation. In addition, the simulation also directly addresses the following question: How does the interaction range influence the MBL phase transition phenomenon? On the other hand, we anticipate that the disorder on long-range interactions is experimentally realizable, e.g. via programmable disorder with trapped $^{171}\text{Yb}^+$ ions [57]. Polar molecules or Rydberg atoms [58], whose positions are randomly distributed in lattices, could also be a candidate system to realize the proposed Ising Hamiltonian in Eq. (1). It should be noted that, the Hamiltonian Eq. (1) has a Z_2 symmetry, i.e. the parity operator $\mathcal{P} = \prod_{1 \leq i \leq L} \sigma_i^x$ commutes with the Hamiltonian. Throughout the paper, unless specified otherwise, all numerical results are obtained from eigenstates with a given parity of $\mathcal{P} = +1$, via exact diagonalization.

In our simulations, we find that, when α is tuned from 0.3 to 3.0, the system shows a drastic change in its global behavior. Even though our numerical study of exact diagonalization suffers from the small system size (up to $L = 14$), our results on the two *sensitive* MBL indicators - the spectral statistics and half-chain entanglement entropy - may contribute to clarify the debate in the proposed phase diagram in the long-range Ising model (see Fig. 1c).

B. The details of numerical calculations

We have defined a dimensionless relative energy as,

$$\epsilon = \frac{E - E_{\min}}{E_{\max} - E_{\min}}, \quad (2)$$

where E_{\min} and E_{\max} are the minimum and maximum energies of the many-body system in a single realization of disorder configuration, respectively. In this work, numerical results are obtained from the 50 eigenstates with their relative energy closest to 59/120, sampled over 1000 different disorder configurations. B is always set to $0.6J$, throughout the paper.

Usually, for simulations of models with long-range interactions, especially for interactions decaying in the form of $R^{-\alpha}$, where $R = |i - j|$ is the distance between two spins of the system at positions i and j , proper scaling factors - such as the Kac prescription [59] - are adapted to ensure that the Hamiltonian satisfies extensiveness property. This is particularly important for the $\alpha < 1$ case since the average energy per spin will diverge as the system goes to the thermodynamic limit (i.e., the size L becomes infinitely large) without such rescaling factor. However, an extra varying parameter renders the analysis of numerical results less clear. To make things even worse, different ways of rescaling might lead to quantitatively different results, even though the qualitative behaviors of the system may not be influenced. Therefore, in this work, no effort is made to guarantee that the model Hamiltonian is extensive. Nevertheless,

the good agreement between our results and the predictions at $0 \leq \alpha \leq 1$ in a previous work using Kac prescription by Hauke and Heyl [42] indicates that the qualitative physics is not changed with or without the Kac prescription.

III. RESULTS AND DISCUSSIONS

A. Spectral statistics

The energy spectral statistics or the statistical energy gap distribution is a sensitive indicator of the MBL phase transition [47]. According to the random matrix theory, because of the overlapping of local freedoms between different eigenstates in a thermalized phase, gaps between adjacent energy levels should obey a Wigner-Dyson distribution, the so-called Gaussian orthogonal ensemble (GOE) in our case. Due to the lack of such overlappings in a localized phase, these gaps instead should follow a Poisson distribution. It is convenient to characterize these two different distributions using the averaged ratio of successive gaps, $\langle r \rangle$ defined by [47]

$$\langle r \rangle = \left\langle \frac{\min \{ \delta_{n+1}, \delta_n \}}{\max \{ \delta_{n+1}, \delta_n \}} \right\rangle, \quad (3)$$

where $\delta_n = E_{n+1} - E_n$ and $\langle \dots \rangle$ denotes an average over some eigenstates calculated within a given disorder realization and over all 1000 different disorder configurations simulated. The GOE distribution has $\langle r \rangle \approx 0.5307(1)$, while the Poisson distribution results in $\langle r \rangle = 2 \ln 2 - 1 \approx 0.3863$ [60]. In the following, these two featured values are denoted by r_G and r_P , respectively.

Typical disorder dependence of the averaged ratio $\langle r \rangle$, as illustrated in Fig. 3, reveals that there is a drastic change when the exponent of the interaction range α is tuned from 0.3 to 3.0. For example, at $\alpha = 0.5$ [see Fig. 3(a)], the ratio decreases monotonically with increasing system size L . It is always smaller than r_G anticipated for a thermalized state. In contrast, at $\alpha = 1.5$ [see Fig. 3(b)], with increasing L the ratio increases at small disorder but decreases at sufficiently large disorder strength. This leads to an apparent crossing point W_c , which locates the critical disorder strength for the MBL phase transition [47]. For the case with $\alpha = 1.5$ in Fig. 3(b), we find that $W_c \approx 6.5$. It is worth emphasizing that all the lines in Fig. 3 approach the Poisson r_P limit at sufficiently large disorder strength, implying that the system is always in MBL phase for strong enough disorder.

By carefully examining the disorder dependence of $\langle r \rangle$ at various exponent of the interaction range, it turns out that $\alpha_c = 1$ is very likely to be the threshold exponent, above and below which the system exhibits entirely different responses at weak disorder. This is evident in Fig. 4 showing the averaged ratio at $\alpha = 1$ in four curves for four different system sizes. We notice that there is no crossing point of these curves. In fact, all these four

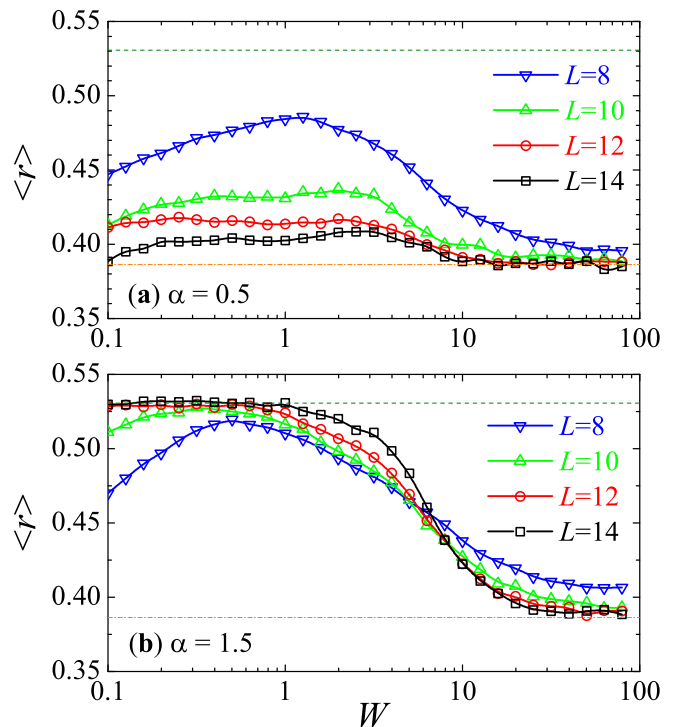


FIG. 3. (color online). The averaged ratio of the adjacent energy spacings $\langle r \rangle$ of the Hamiltonian Eq. (1) at $\alpha = 0.5$ (a) and $\alpha = 1.5$ (b) for four different lengths $L = 8, 10, 12$ and 14 . The dashed and dot-dashed lines indicate $r_G \approx 0.5307(1)$ and $r_P \approx 0.3863$, respectively.

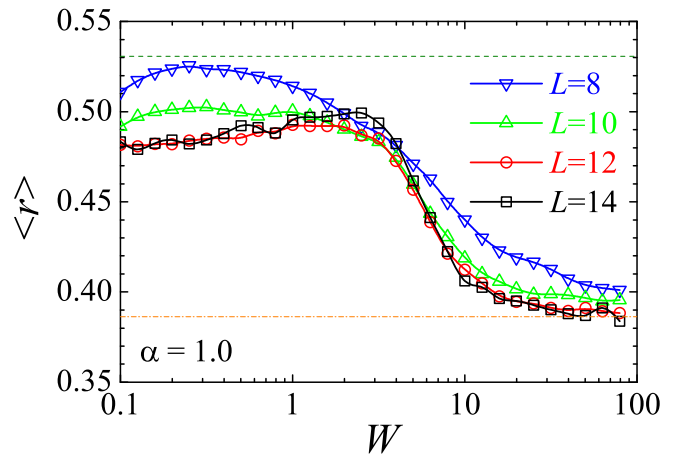


FIG. 4. (color online). The averaged ratio of the adjacent energy spacings $\langle r \rangle$ of the Hamiltonian Eq. (1) at $\alpha = 1$.

curves are nearly tangent with each other at $W \approx 3.5$. Therefore, it is reasonable to assume the following phase structure:

- For $\alpha < 1$, the system is mostly localized for nonzero disorder strength. But, there are probably two kinds of localized phases, separated by a quantum critical region; and

- For $\alpha > 1$, in the small limit of disorder strength, the system is in the thermalized phase that satisfies ETH, while in the strong disorder limit, the system is in the MBL localized phase. These two phases are connected via an MBL phase transition.

These phase diagram structure are confirmed by studying another popular indicator: quantum entanglement entropy.

B. Entanglement Entropy

The entanglement entropy S_E has been widely used in the literature [10, 14, 15, 27, 28, 48, 61] to characterize the MBL. The meaning and implication of this indicator is clear. One of the most important features of MBL (as is indicated by its name) is localization. Local freedoms in an MBL eigenstate are no longer entangled with freedoms that are far away in real space. Thus, the entanglement entropy of a subsystem should follow an area law deeply in MBL phase rather than the volume law found in equilibrated states. Specifically, for our Hamiltonian, the half-chain entanglement entropy deeply in MBL phase should be independent of the length of the system and very close to $\ln 2$. The origin of the $\ln 2$ is due to the Z_2 parity symmetry. A detailed explanation is given in Appendix A.

The effective temperature for an eigenstate with energy E_{eig} can be defined as:

$$E_{eig} = \frac{\text{Tr}(\mathcal{H}e^{-\beta\mathcal{H}})}{\text{Tr}(e^{-\beta\mathcal{H}})}, \quad (4)$$

where $\beta = 1/k_B T$ with k_B being the Boltzmann constant and T effective temperature.

In this work, we are focusing on eigenstates with relative energy close to $59/120$, whose effective temperature should therefore be very close to infinity. Thus, in thermal phases, the half-chain entanglement entropy should be close to $(L \ln 2 - 1)/2$, the classical entropy of the half chain at infinite temperature [62]. Also, as is implied by the Eq. (4), the relative position of an eigenstate in the energy spectrum can drastically influence its effective temperature. Under the assumption that it is the portion of the averaged spectrum rather than the absolute number of the eigenstates that matters for the structure of entanglement entropy, we calculate the entanglement entropy of different numbers of eigenstates for Hamiltonians with different spin numbers to ensure that the averaged eigenstates occupy a constant portion of the whole spectrum. Specifically, for chains with 8, 10 and 12 spins, the entanglement entropy S_E and uncertainty δS_E are calculated by using 3, 12 and 48 eigenstates with relative energy closest to $59/120$ respectively. In principle, we should have used 192 eigenstates for a chain with 14 spins, but the calculation turned out to be too heavy and time-consuming. Thus, results of chain with 14 spins are calculated using only 50 eigenstates with relative energy

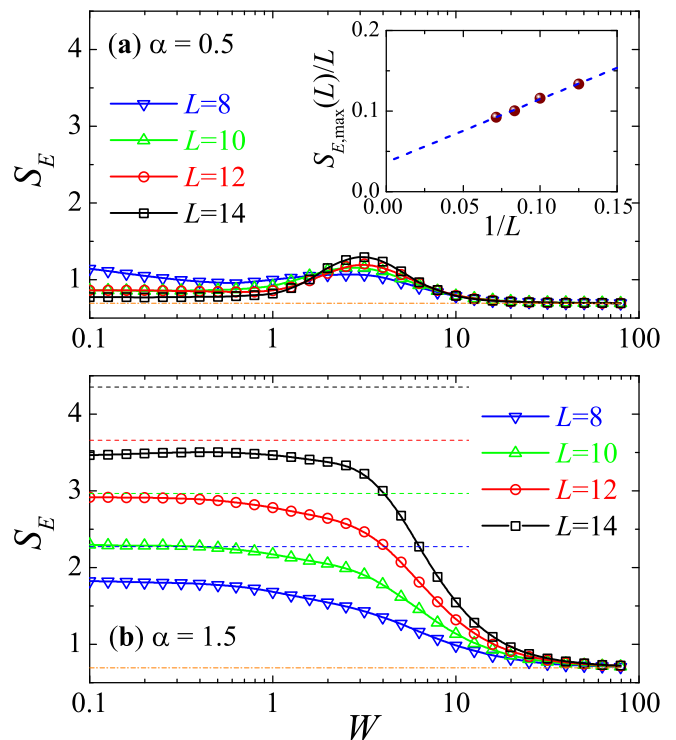


FIG. 5. (color online). The half-chain entanglement entropy S_E of the Hamiltonian Eq. (1) at $\alpha = 0.5$ (a) and $\alpha = 1.5$ (b) for four different lengths $L = 8, 10, 12$ and 14 . The thin dot-dashed lines in both subplots indicate the $\ln 2$ entropy anticipated in the deep MBL phase and the dashed lines in (b) indicate the expected classical entropy $(L \ln 2 - 1)/2$ in thermalized phase. The inset in (a) shows the maximum entropy per spin (found at the intermediate disorder strength) as a function of $1/L$.

closed to $59/120$. Nevertheless, the result of the chain with 14 spins still shows a similar pattern as those shorter chains, indicating our choice is acceptable.

Our numerical simulations shows that the exponent α of the interaction range drastically changes the behavior of the entanglement entropy. As can be seen clearly in Fig. 5(a), in the $\alpha = 0.5$ case, the half-chain entanglement entropy at both weak and strong disorder strengths is largely independent on the length of the system and always lies very close to $\ln 2$. This observation seems to be consistent with the earlier prediction by Hauke and Heyl [42], which states that for $\alpha < 1$ the disordered Ising chain is always localized for any finite disorder strength. However, at the intermediate disorder strength, the entanglement entropy also shows a pronounced peak structure, with a maximum entropy that increases with increasing system size. A close examination of the size dependence is given in the inset of Fig. 5(a). We find that the maximum entropy per spin, $S_E(L)/L$, scales to a finite value ($\approx 0.04 \ll 0.5 \ln 2$) in the thermodynamic limit of $L \rightarrow \infty$. Thus, the maximum entropy seems to follow a *weak* volume law, instead of the area law obeyed in the localized phase. Therefore, there is a possibility

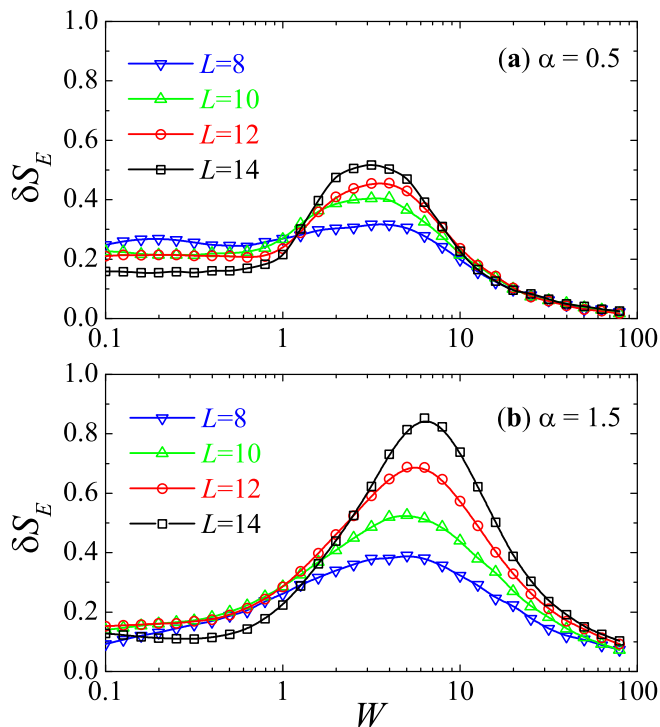


FIG. 6. (color online). The uncertainty of the half-chain entanglement entropy δS_E of the Hamiltonian Eq. (1) at $\alpha = 0.5$ (a) and $\alpha = 1.5$ (b) for four different lengths $L = 8, 10, 12$ and 14 .

that, at $\alpha = 0.5$, two different MBL phases may exist at weak and strong disorder strengths, respectively. They are separated by a quantum critical region at intermediate disorder strength, in which the entanglement entropy follows a weak volume law. At $\alpha = 1.5$, Fig. 5(b) shows that the entanglement entropy has a linear dependence on the system size at weak disorder strength and approaches $\ln 2$ at strong disorder strength. This behavior was found earlier in a disordered spin chain with nearest-neighbor interactions [13, 26], where a phase transition from a thermalized state to the MBL phase is now well established.

The above picture is further supported by the behavior of the uncertainty of the entanglement entropy δS_E , as shown in Fig. 6. For the $\alpha = 1.5$ case in Fig. 6(b), in the small disorder limit, the uncertainty is small, consistent with the fact that the system is in a thermal state and hence the half-chain entanglement entropy should approach the constant classical limit. In the strong disorder limit, the uncertainty also gradually decreases to zero, in agreement with the fact that the system is localized and thus its half-chain entanglement entropy approaches the constant value of $\ln 2$. At intermediate disorder strength, the half-chain entanglement entropy of the eigenstates can be either close to $\ln 2$ or extensively large, leading to a large uncertainty, which can be viewed as an excellent signature of the MBL phase transition.

For the $\alpha = 0.5$ case in Fig. 6(a), on the other hand,

the system is mostly in the exotic localized states, as we mentioned earlier. It becomes non-trivial to predict the behavior of the uncertainty of the entanglement entropy. Nevertheless, because the entanglement entropy itself is small and nearly independent on the length of the chain, we anticipate a small uncertainty, which is indeed seen in Fig. 6(a) at both weak and strong disorder strengths. The peak structure of the uncertainty at intermediate disorder strength also seems to be consistent with the weak volume law of the entanglement entropy discussed earlier. Similar to the $\alpha = 1.5$ case, we may regard it as the indication of a possible phase transition between two MBL phases.

To confirm that the proposed phase diagram structure is qualitatively correct in the thermodynamic limit, we now turn to perform a finite size scaling.

C. Finite size scaling

The data we used for performing the finite size scaling analysis are the half-chain entanglement entropy S_E and the related uncertainty δS_E . By suitably defining a scaled disorder strength and scaled S_E and δS_E , we anticipate that all the data with different system sizes will collapse onto a single curve near possible quantum phase transition. Through data collapse, one may be able to extract useful information about the phase transition and determine the critical disorder strength. Unfortunately, currently we do not have a well-established theory to provide us with the reliable scaling form yet. Thus, in this work, we adapt the most popular scaling form used in the previous studies [13],

$$Q(L, W) = g(L) f \left[(W - W_c) L^{1/\nu} \right], \quad (5)$$

where Q stands for S_E or δS_E and $g(L) = [(L - 2) \ln 2 - 1]/2$ is the difference between the two limiting entropies in the thermalized phase and in the MBL phase. It is used as a pre-factor to rescale the entanglement entropy and the related uncertainty. ν is known as the critical exponent and W_c is the critical disorder strength. Both of them are treated as the variational parameters, in order to scale the data with different L onto a single scaling curve $f(x)$.

In Fig. 7 and Fig. 8, we present the scaled entanglement entropy and its uncertainty at $\alpha = 0.5$ and $\alpha = 1.5$, respectively. By suitably adjusting the two parameters ν and W_c , the originally scattered data of S_E (in Fig. 5) or δS_E (in Fig. 6) indeed collapse onto a single curve, as one may anticipate. The data collapse at $\alpha = 1.5$ is particularly satisfactory, confirming the existence of a MBL phase transition. This conclusion disagrees with a previous prediction from the resonant spin-pair excitations argument that a disordered transverse-field Ising chain should always be delocalized for $1 < \alpha < 2$ [51].

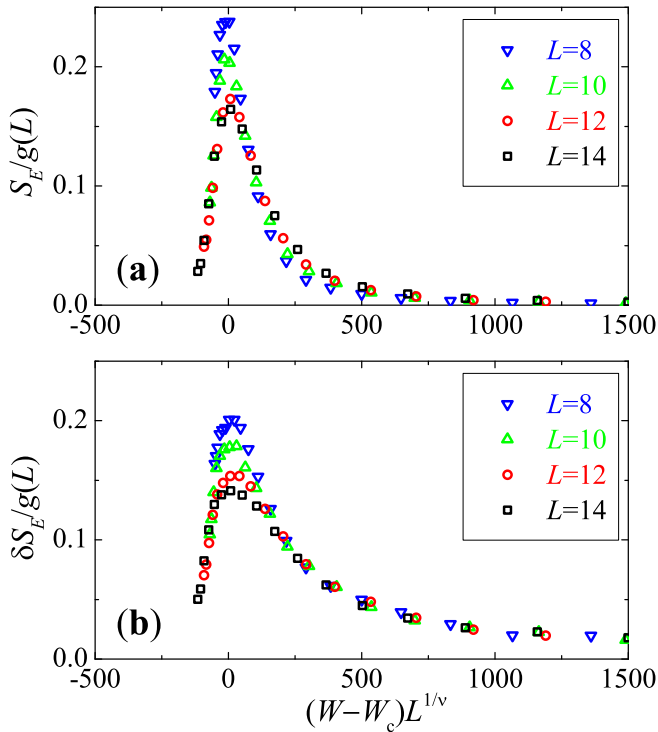


FIG. 7. (color online). The entanglement entropy and its uncertainty, in units of $g(L) = [(L-2) \ln 2 - 1]/2$, as a function of the scaled disorder strength $(W - W_c)L^{1/\nu}$ at $\alpha = 0.5$.

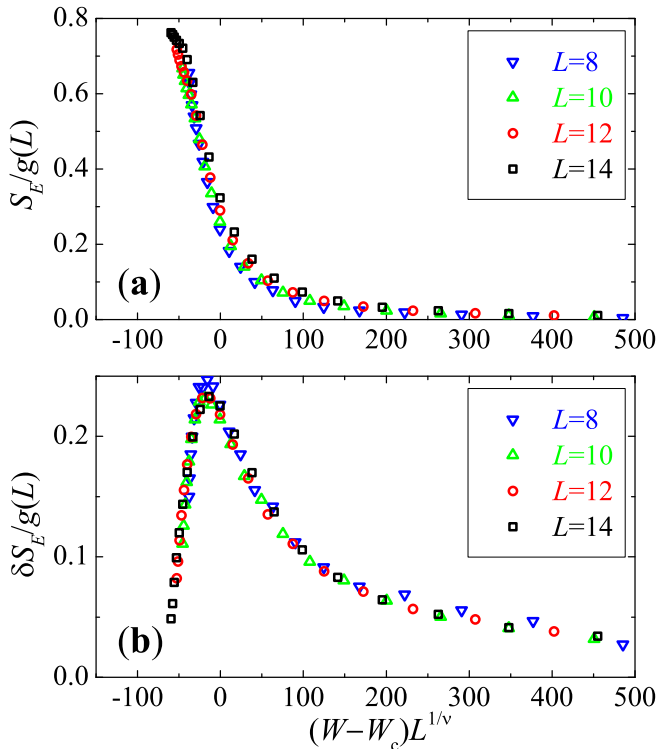


FIG. 8. (color online). The entanglement entropy and its uncertainty, in units of $g(L)$, as a function of the scaled disorder strength $(W - W_c)L^{1/\nu}$ at $\alpha = 1.5$.

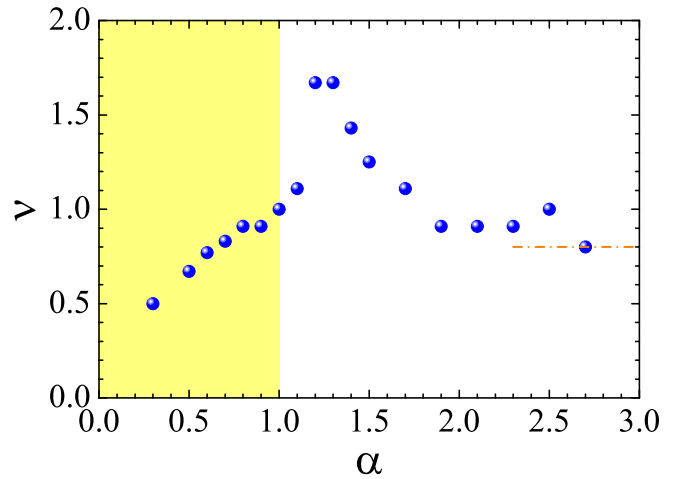


FIG. 9. (color online). The critical exponent ν of the Hamiltonian Eq. (1) as a function of the exponent of the interaction range α . The dot-dashed line indicates the result of a disordered Heisenberg chain with nearest-neighbor interactions, $\nu = 0.80 \pm 0.04$ [13].

D. Phase diagram

Finally, we performed the finite size scaling at different exponent of the interaction range α . The resulting critical disorder strengths and critical exponents are shown in the phase diagram Fig. 2 (circles) and Fig. 9, respectively. To obtain the critical disorder strength, we have also used the averaged gap ratio $\langle r \rangle$ and extract the position of the cross point, see for example, Fig. 3(b). This is another useful way valid down to $\alpha = 1$. In the phase diagram Fig. 2, the critical disorder strengths determined using $\langle r \rangle$ are plotted by diamond symbols. In general, the phase boundary determined from the two methods coincides well. This suggests that for our model Hamiltonian Eq. (1), the averaged ratio of successive gaps and the finite-size scaling analysis of the entanglement entropy as well as its uncertainty are the equivalent methods to pinpoint the phase transition.

For the critical exponent, as shown in Fig. 9, there is a peak around $\alpha = 1$. This is a strong indication that $\alpha_c = 1$ is a threshold exponent, which separates the phase diagram Fig. 2 into two parts. When α is small, the critical exponent trends to 0.5. When α is large, the critical exponent seems to saturate to 0.9, a value that is close to the critical exponent obtained for a disordered Heisenberg chain with nearest-neighbor interactions at the same infinite temperature, i.e., $\nu = 0.80 \pm 0.04$ [13]. This is understandable, since, as the exponent of the interaction range α goes to infinity, the long-range interaction in our model Hamiltonian Eq. (1) is naturally reduced to a short-range interaction.

IV. SUMMARY

In conclusions, we have investigated a one-dimensional Ising spin model with random long-range interactions, a system that may be relevant to trapped ions, Rydberg atoms and polar molecules in cold-atom experiments. By systematically studying the two many-body localization indicators such as the averaged ratio of successive energy gaps and the entanglement entropy (and its uncertainty), and performing the finite size scaling, we have found that the system always experiences a many-body localization phase transition at sufficiently large disorder strength. To some extent, this is a surprising result, as the previous theoretical investigation suggested a complete delocalization at the exponent of the interaction range $1 < \alpha < 2$, due to the picture of resonant spin-pair excitations [51]. A phase diagram has been determined (see Fig. 2), as functions of the disorder strength W and the interaction exponent α . We have determined the phase boundary and have found that $\alpha_c = 1$ is a threshold interaction exponent. For $\alpha > 1$, the system undergoes a thermal-MBL phase transition with increasing disorder strength; while for $\alpha < 1$, the system is mostly many-body localized, a result in agreement with a previous finding [42]. There could be two different localized phases, separated by a quantum critical region, whose properties are yet to be understood.

ACKNOWLEDGMENTS

This work was supported by the Australian Research Council (ARC) Future Fellowship grants (Grant Nos. FT140100003 and FT130100815) and Discovery Projects (Grant Nos. DP140100637 and DP140103231). All the numerical calculations were performed using Swinburne new HPC resources (Green II) at Swinburne University of Technology.

Appendix A: The origin of $\ln 2$ entanglement entropy in the deep MBL phase

As mentioned and demonstrated in Section III, deeply in the MBL phase the half chain entanglement entropy approaches $\ln 2$ in the large disorder limit. This $\ln 2$ entropy originates from the Z_2 parity symmetry of the Hamiltonian. To prove this, let us consider the half chain entanglement entropy of other two Hamiltonians under similar parameters and conditions,

$$\mathcal{H}_1 = J \sum_{1 \leq i < j \leq L} \frac{1}{|j-i|^\alpha} \sigma_i^z \sigma_j^z + J \sum_{i=1}^L h_i \sigma_i^x, \quad (\text{A1})$$

$$\mathcal{H}_2 = J \sum_{1 \leq i < j \leq L} \frac{1 + h_i h_j}{|j-i|^\alpha} \sigma_i^z \sigma_j^z + B \sum_{i=1}^L \sigma_i^x + C \sum_{i=1}^L \sigma_i^z, \quad (\text{A2})$$

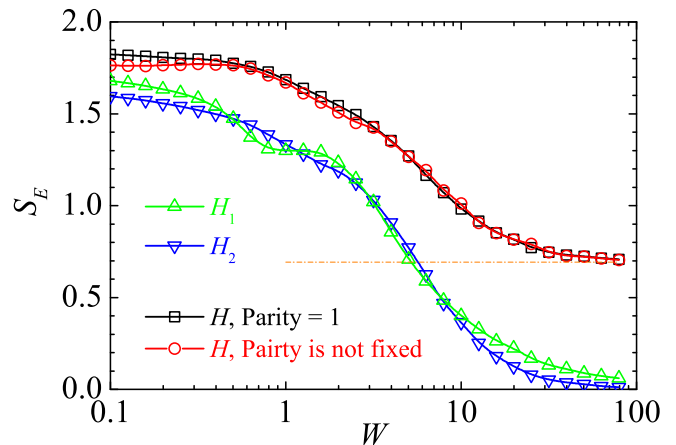


FIG. 10. The half chain entanglement entropy S_E of different model Hamiltonians at $\alpha = 1.5$ and $L = 8$. The thin dot-dashed line indicates the $\ln 2$ entanglement entropy observed in the deep MBL regime for the model Hamiltonian \mathcal{H} .

where h_i is the dimensionless random variable drawn from the uniform distribution in the domain $[-W, W]$. The Hamiltonian \mathcal{H}_1 is simply the random transverse-field Ising model considered earlier by Hauke and Heyl [42] and by Burin [51]. In the Hamiltonian \mathcal{H}_2 , a longitudinal field is applied. Both \mathcal{H}_1 and \mathcal{H}_2 break the Z_2 parity symmetry. To be specific, we consider the case with $\alpha = 1.5$ and $L = 8$.

The half-chain entanglement entropies of three eigenstates with relative energy closest to $1/2$ (for \mathcal{H}_1) and $59/120$ (for \mathcal{H}_2) are calculated and averaged over 1000 different disorder configurations. To ensure that the comparison is carried out under similar conditions, in the Hamiltonian \mathcal{H}_2 , B is set to $0.6J$ as before, while C is taken to be $0.01J$. We also consider the Hamiltonian Eq. (1) *without* imposing the parity constraint of $\mathcal{P} = +1$.

In Fig. 10, we compare the half-chain entanglement entropies of four different situations: \mathcal{H}_1 (up triangles), \mathcal{H}_2 (down triangles), \mathcal{H} with the Z_2 parity $\mathcal{P} = +1$ (squares), and \mathcal{H} without the parity constraint (circles). It is clear that, as soon as the Z_2 parity symmetry is broken, no matter it is destroyed by a disordered transverse field or by a uniform longitudinal field, deeply in the localized phase, the entanglement entropy goes to zero. On the other hand, the parity constraint implemented in our calculations (as in the main text) has essentially no quantitative influence on the entanglement entropy. This is understandable since the model Hamiltonian respects the Z_2 parity symmetry and then, in principle, the eigenstates solved by exact diagonalization would have a deterministic parity. With nearly the same energy, these eigenstates (having either $\mathcal{P} = +1$ or $\mathcal{P} = -1$) would have nearly the same entanglement entropy.

However, there are two main reasons that renders the implementation of the parity constraint preferable. Firstly, when the disorder strength is very large, all the eigenstates of the Hamiltonian \mathcal{H} become nearly doubly

degenerate, due to the Z_2 parity symmetry. Our results are all calculated using Matlab via its 'eigs' function. Due to the limitation of its inherent algorithm, this function can not precisely distinguish two nearly degenerate eigenstates. If a parity is not settled from the beginning,

it will produce non-physical entanglement entropy due to the parity mixing. On the other hand, the use of a deterministic parity can reduce the dimension of the Hilbert space by half. This is highly preferable in numerical simulations.

-
- [1] D. M. Basko, I. L. Aleiner, and B. L. Altshuler, *Ann. Phys. (N.Y.)* **321**, 1126 (2006).
- [2] R. Nandkishore and D. A. Huse, *Annu. Rev. Condens. Matter Phys.* **6**, 15 (2015).
- [3] E. Altman and R. Vosk, *Annu. Rev. Condens. Matter Phys.* **6**, 383 (2015).
- [4] J. W. Gibbs, *Transactions of the Connecticut Academy*, **3**, 108 (1878).
- [5] C. C. Moore, *Proc. Natl. Acad. Sci.* **112**, 1907 (2015).
- [6] J. V. Neumann, *Proc. Natl. Acad. Sci.* **18**, 70 (1932).
- [7] J. V. Neumann, *Proc. Natl. Acad. Sci.* **18**, 263 (1932).
- [8] M. Srednicki, *Phys. Rev. E* **50**, 888 (1994).
- [9] M. Rigol and M. Srednicki, *Phys. Rev. Lett.* **108**, 110601 (2012).
- [10] B. Zhao, *Eigenstate Phase Transitions*, Ph.D. thesis, Princeton University (2015).
- [11] P. W. Anderson, *Phys. Rev.* **109**, 1492 (1958).
- [12] F. Evers and A. D. Mirlin, *Rev. Mod. Phys.* **80**, 1355 (2008).
- [13] D. J. Luitz, N. Laflorencie, and F. Alet, *Phys. Rev. B* **91**, 081103 (2015).
- [14] E. Baygan, S. P. Lim, and D. N. Sheng, *Phys. Rev. B* **92**, 195153 (2015).
- [15] X. Li, S. Ganeshan, J. H. Pixley, and S. Das Sarma, *Phys. Rev. Lett.* **115**, 186601 (2015).
- [16] T. C. Berkelbach and D. R. Reichman, *Phys. Rev. B* **81**, 224429 (2010).
- [17] D. Pekker, G. Refael, E. Altman, E. Demler, and V. Oganesyan, *Phys. Rev. X* **4**, 011052 (2014).
- [18] K. Agarwal, S. Gopalakrishnan, M. Knap, M. Müller, and E. Demler, *Phys. Rev. Lett.* **114**, 160401 (2015).
- [19] R. Nandkishore, S. Gopalakrishnan, and D. A. Huse, *Phys. Rev. B* **90**, 064203 (2014).
- [20] D. A. Huse, R. Nandkishore, V. Oganesyan, A. Pal, and S. L. Sondhi, *Phys. Rev. B* **88**, 014206 (2013).
- [21] B. Bauer and C. Nayak, *J. Stat. Mech.*, P09005 (2013).
- [22] Y. Bahri, R. Vosk, E. Altman, and A. Vishwanath, *Nat. Commun.* **6**, 7341 (2015).
- [23] A. Chandran, V. Khemani, C. R. Laumann, and S. L. Sondhi, *Phys. Rev. B* **89**, 144201 (2014).
- [24] R. Vosk and E. Altman, *Phys. Rev. Lett.* **112**, 217204 (2014).
- [25] T. P. Marko Znidaric and P. Prelovsek, *Phys. Rev. B* **77**, 064426 (2008).
- [26] J. A. Kjäll, J. H. Bardarson, and F. Pollmann, *Phys. Rev. Lett.* **113**, 107204 (2014).
- [27] M. Serbyn, Z. Papić, and D. A. Abanin, *Phys. Rev. Lett.* **111**, 127201 (2013).
- [28] J. H. Bardarson, F. Pollmann, and J. E. Moore, *Phys. Rev. Lett.* **109**, 017202 (2012).
- [29] R. Vosk and E. Altman, *Phys. Rev. Lett.* **110**, 067204 (2013).
- [30] M. Serbyn, Z. Papić, and D. A. Abanin, *Phys. Rev. Lett.* **110**, 260601 (2013).
- [31] C. Gogolin, M. P. Müller, and J. Eisert, *Phys. Rev. Lett.* **106**, 040401 (2011).
- [32] I. Bloch, J. Dalibard, and W. Zwerger, *Rev. Mod. Phys.* **80**, 885 (2008).
- [33] C. Chin, R. Grimm, P. Julienne, and E. Tiesinga, *Rev. Mod. Phys.* **82**, 1225 (2010).
- [34] I. Bloch, *Nat. Phys.* **8**, 267 (2012).
- [35] M. Schreiber, S. S. Hodgman, P. Bordia, H. P. Lueschen, M. H. Fischer, R. Vosk, E. Altman, U. Schneider, and I. Bloch, *Science* **349**, 842 (2015).
- [36] P. Bordia, H. P. Luschen, S. S. Hodgman, M. Schreiber, I. Bloch, and U. Schneider, *Phys. Rev. Lett.* **116**, 140401 (2016).
- [37] J.-y. Choi, S. Hild, J. Zeiher, P. Schauss, A. Rubio-Abadal, T. Yefsah, V. Khemani, D. A. Huse, I. Bloch, and C. Gross, *Science* **352**, 1547 (2016).
- [38] J. Smith, A. Lee, P. Richerme, B. Neyenhuis, P. W. Hess, P. Hauke, M. Heyl, D. A. Huse, and C. Monroe, "Many-body localization in a quantum simulator with programmable disorder," (2015), arXiv:1508.07026.
- [39] V. Ros, M. Mueller, and A. Scardicchio, *Nucl. Phys. B* **891**, 420 (2014).
- [40] N. Y. Yao, C. R. Laumann, S. Gopalakrishnan, M. Knap, M. Müller, E. A. Demler, and M. D. Lukin, *Phys. Rev. Lett.* **113**, 243002 (2014).
- [41] C. R. Laumann, A. Pal, and A. Scardicchio, *Phys. Rev. Lett.* **113**, 200405 (2014).
- [42] P. Hauke and M. Heyl, *Phys. Rev. B* **92**, 134204 (2015).
- [43] C. Karrasch and J. E. Moore, *Phys. Rev. B* **92**, 115108 (2015).
- [44] R. Vosk, D. A. Huse, and E. Altman, *Phys. Rev. X* **5**, 031032 (2015).
- [45] A. C. Potter, R. Vasseur, and S. A. Parameswaran, *Phys. Rev. X* **5**, 031033 (2015).
- [46] S. P. Lim and D. N. Sheng, *Phys. Rev. B* **94**, 045111 (2016).
- [47] V. Oganesyan and D. A. Huse, *Phys. Rev. B* **75**, 155111 (2007).
- [48] A. Pal and D. A. Huse, *Phys. Rev. B* **82**, 174411 (2010).
- [49] A. D. Luca and A. Scardicchio, *Europhys. Lett.* **101**, 37003 (2013).
- [50] M. Serbyn and J. E. Moore, *Phys. Rev. B* **93**, 041424 (2016).
- [51] A. L. Burin, *Phys. Rev. B* **91**, 094202 (2015).
- [52] A. L. Burin, *Phys. Rev. B* **92**, 104428 (2015).
- [53] E. Canovi, D. Rossini, R. Fazio, G. E. Santoro, and A. Silva, *Phys. Rev. B* **83**, 094431 (2011).
- [54] M. Pino, *Phys. Rev. B* **90**, 174204 (2014).
- [55] Y.-L. Wu and S. Das Sarma, *Phys. Rev. A* **93**, 022332 (2016).
- [56] Y. Bar Lev, G. Cohen, and D. R. Reichman, *Phys. Rev. Lett.* **114**, 100601 (2015).
- [57] K. Kim, S. Korenblit, R. Islam, E. E. Edwards, M.-S. Chang, C. Noh, H. Carmichael, G.-D. Lin, L.-M.

- Duan, C. C. J. Wang, J. K. Freericks, and C. Monroe, *New J. Phys.* **13**, 105003 (2011).
- [58] X. Deng, B. L. Altshuler, G. V. Shlyapnikov, and L. Santos, *Phys. Rev. Lett.* **117**, 020401 (2016).
- [59] L. B. Ioffe and M. Mézard, *Phys. Rev. Lett.* **105**, 037001 (2010).
- [60] Y. Y. Atas, E. Bogomolny, O. Giraud, and G. Roux, *Phys. Rev. Lett.* **110**, 084101 (2013).
- [61] T. Grover, “Certain general constraints on the many-body localization transition,” (2014), arXiv:1405.1471.
- [62] D. N. Page, *Phys. Rev. Lett.* **71**, 1291 (1993).